

## IV.A.7 Characterization of Atomic and Electronic Structure of Electrochemically Active SOFC Cathode Surfaces

Meilin Liu (Primary Contact), YongMan Choi,  
Robert Williams, Jr.

Georgia Institute of Technology  
771 Ferst Drive NW  
Atlanta, GA 30332  
Phone: (404) 894-6114; Fax: (404) 894-9140  
E-mail: meilin.liu@mse.gatech.edu

DOE Project Manager: Lane Wilson  
Phone: (304) 285-1336  
E-mail: Lane.Wilson@netl.doe.gov

the complexity of the involved charge and mass transfer processes, however, it is extremely difficult to probe the mechanistic details using experimental tools. Here we report our findings on the application of periodic density functional theory (DFT) calculations, containing the exploration of the molecular processes involved in oxygen reduction on  $\text{LaMnO}_3$ -based cathode surfaces. We aim to predict the most probable oxygen reaction pathway as well as the vibrational frequencies of the adsorbed surface oxygen species. To develop a reliable experimental approach for the determination of the surface catalytic properties of various cathode materials, we have designed, fabricated, and characterized dense LSM-GDC composite electrodes.

### Objectives

- Elucidate oxygen reduction mechanisms on  $\text{LaMnO}_3$ -based cathode materials using quantum chemical calculations
- Simulate the interactions between  $\text{O}_2$  and  $\text{LaMnO}_3$ -based cathode materials under solid oxide fuel cell (SOFC) operating conditions using quantum molecular dynamics (QMD) methods
- Fabricate, characterize, and model dense  $\text{La}_{0.85}\text{Sr}_{0.15}\text{MnO}_3$  (LSM)- $\text{Ce}_{0.9}\text{Gd}_{0.1}\text{O}_{1.95}$  (GDC) composite electrodes, which will be used as a platform for characterization of surface catalytic properties of other cathode materials

### Accomplishments

- Quantum chemical calculations showed that the oxygen reduction reaction on  $\text{LaMnO}_3$ -based cathode materials may occur via a stepwise elementary reaction sequence.
- QMD simulations predict that defective  $\text{LaMnO}_3$  exhibits faster  $\text{O}_2$  dissociation kinetics than perfect  $\text{LaMnO}_3$  at  $800^\circ\text{C}$ , suggesting that oxygen vacancies play a critical role in oxygen reduction reactions.
- Fabricated and characterized dense LSM-GDC composite electrodes with various composition and microstructures. The amount of triple-phase boundaries (TPBs) was determined using stereological methods.

---

### Introduction

Understanding the detailed oxygen reduction mechanism is critical to achieving a rational design of new cathode materials for SOFCs [1,2,3]. Because of

### Approach

Periodic DFT calculations [4,5] and molecular dynamics (MD) simulations have been used to examine oxygen reduction reactions and ionic transport of cathode materials for SOFCs. The details of the computational methods are as described elsewhere [2,3,6].

A dense LSM-GDC composite electrode is typically fabricated with a GDC electrolyte layer to form a bi-layer structure using a co-pressing and co-firing process. LSM (Rhodia, average particle size:  $1.1\ \mu\text{m}$ ) and GDC (Rhodia, average particle size:  $0.3\ \mu\text{m}$ ) powders with various volume ratios ranging from 40:60 to 70:30 were mixed in a mortar further reducing particle sizes. The co-pressing consisted of several successive steps: the as-prepared mixture powder was added to a die (diameter of 10 mm) and tapped smooth using a pestle. Next, GDC powder was loaded into the die. The whole body was cold-pressed under 200 MPa into cylindrical pellets using a uniaxial die-press. After firing the samples at  $1,450^\circ\text{C}$  for 5 h in air, dense GDC/LSM-GDC wafers were attained. The thicknesses of GDC and LSM-GDC composite were  $\sim 0.5\ \text{mm}$  and  $\sim 0.15\ \text{mm}$ , respectively.

### Results

Shown in Figure 1a are the optimized geometries, O-O bonds, and their vibrational frequencies of the adsorbed oxygen species on a defective  $\text{LaMnO}_3$  (with an oxygen vacancy). Those intermediates on the defective  $\text{LaMnO}_3$  surface are energetically more favorable compared to those on a perfect surface (without oxygen vacancy). We carried out a mechanistic study for the molecular adsorption pathway at the defective  $\text{LaMnO}_3$  surface. Since we were unable to locate peroxo-like species at the La cation site, we

considered only the Mn cation pathway. As depicted in Figure 1b, the first step is the formation of either superoxo-like **Mn-super** or peroxy-like **Mn-per** with exothermicities of 1.82 or 2.70 eV, respectively. As summarized in Figure 1a, they have distinct vibrational frequencies of 1265 or 861  $\text{cm}^{-1}$ , respectively. Because of the further charge transfer from the surface to the adsorbate, superoxo-like **Mn-super** can also isomerize to the peroxy-like **Mn-per** intermediate after overcoming a 0.1 eV reaction barrier of **TS**, leading to a lengthening of the O-O bond distance from 1.301 to 1.445 Å (see Figure 1a). Then, one of the oxygen atoms of the peroxy-like **Mn-per** species is incorporated into the oxygen vacancy ( $V_{\text{O}}^{\bullet\bullet}$ ), while breaking the O-O bond without a well-defined transition state, producing **P-V** with an exothermicity of 6.99 eV. The highly exothermic process validates the good catalytic activity for oxygen dissociation on  $\text{LaMnO}_3$ -based cathode materials. The monatomic oxygen species absorbed at the Mn cation diffuses to a more stable site (labeled as Products in Figure 1), which is 2.32 eV more stable than **P-V**. In order to simulate SOFC conditions on the  $\text{LaMnO}$ -terminated  $\text{LaMnO}_3$  surface models, MD simulations at  $800^\circ\text{C}$  were carried out. To simulate a reactant gas-phase oxygen, the distance between an  $\text{O}_2$  molecule and the surface was kept at approximately 4 Å and fully optimized. The defective  $\text{LaMnO}_3$  surface was modeled to verify our minimum-energy paths (MEPs) shown in Figure 1b. For the MD simulations,  $\Delta t = 2$  femtoseconds (fs) was applied and the calculations were iterated until they reached an equilibrium state. As illustrated in Figure 2, in 100 fs, the molecular adsorption of a superoxo-like species occurs. Then, one of the oxygen atoms of the adsorbed species moves toward the oxygen vacancy with energy stabilization and charge transfer, which takes place in approximately 130 fs. After the incorporation process in an additional 30 fs, the adsorbed oxygen monatomic species at Mn cations diffuses to a more stable site. The time from adsorption to dissociation (with incorporation) was 220 fs. Even though MEP calculations (Figure 1b) determined two pathways via superoxo- and peroxy-like species without a reaction barrier, the MD simulations with our surface models suggested that the most probable reaction pathway is the formation of superoxo-like species, and then conversion to peroxy-like species with a small reaction barrier. Thus, we can write a possible route with oxygen vacancies on the  $\text{LaMnO}_3$ -based surfaces. We summarize the most probable pathway for the oxygen-reduction mechanism based on the DFT/MD modeling

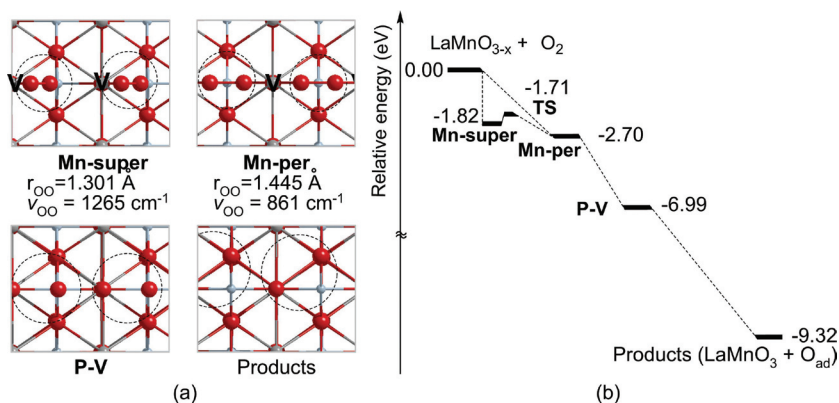


**FIGURE 1.** (a) Geometrical information of adsorbed oxygen species on a defective  $\text{LaMnO}_3$  surface. **V** and dashed circles denote an oxygen vacancy and adsorbed oxygen species on the surface, respectively. (b) Potential energy profiles at 0 K for the oxygen reduction reaction on a defective  $\text{LaMnO}_3$  surface.

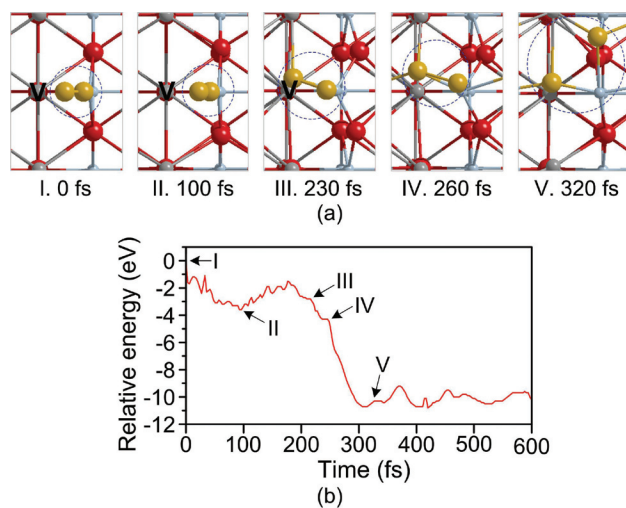


**FIGURE 2.** MD results simulated at  $800^\circ\text{C}$ . **V** and dashed circles denote an oxygen vacancy and adsorbed oxygen species on the surface, respectively.

in Figure 3, where (g), (ad), (super), (per), and (lc) represent gas, molecular adsorption, superoxo-like species, peroxy-like species, and lattice, respectively.

Shown in Figure 4a is a typical scanning electron microscope (SEM) micrograph of the dense composite layer. After performing energy dispersive X-ray (EDX) characterization on hundreds of small particles, it was found that particles with a terrace structure on their surface corresponded to LSM, while those with small dents on their surface corresponded to GDC. In this manner, the two phases were able to be differentiated. To quantify the TPB length for the various sample sets, established stereographic techniques were employed. Micrographs of the sample surfaces were taken using SEM and test lines were overlaid on the image. Using the known magnification of the micrograph, the

actual total length of the test lines was determined. The number of intersections between the test lines and the LSM-GDC grain boundaries (which represents a TPB line),  $P_L$ , were counted. This process was repeated at different locales on the surfaces of several samples for a minimum of thirty fields of view, and an average value of the number of intersections per test line,  $\langle P_L \rangle$ , was calculated. The average value of the total boundary length per unit area,  $\langle L_A \rangle$ , is related to  $\langle P_L \rangle$  through the simple expression,  $\langle L_A \rangle = \pi/2 \langle P_L \rangle$ . Figure 4b shows a plot of inverse polarization resistance versus TPB lengths. The plot is expected to be linear but shows significant scatter, specifically from the low volume percentages of LSM samples. The main cause of this nonlinearity is due most likely to not all of the TPBs for each sample being active. For the TPB around each LSM particle to be considered active, it must contact a GDC particle that is part of a percolating cluster through to the electrolyte. The likelihood of percolation for the GDC particles becomes increasingly smaller as the volume percentage of LSM increases. It is expected that once site percolation is taken into account and the amount of active TPB length is calculated, better linearity will be achieved.

## Conclusions and Future Directions

In the past year, we have made important progress in elucidation of the mechanisms of oxygen reduction of perovskite-type cathode materials for SOFCs using quantum chemical calculations. Dense LSM-GDC composite electrodes have been developed using a co-pressing and co-firing technique. The amount of TPB length for samples of varying volume percentages was determined using stereographic methods. It was found that the volume percentage of 50% LSM to 50% GDC produced the largest amount of TPB length. In correlating the cell performance with the TPB length, a large amount of scatter in the data was observed. Future studies are briefly outlined as follows:

- The computational framework will be used to predict new cathode material with fast  $O_2$  reduction kinetics and rapid ionic transport. Once a candidate material is identified, we will use experimental methods to characterize the catalytic and transport properties.

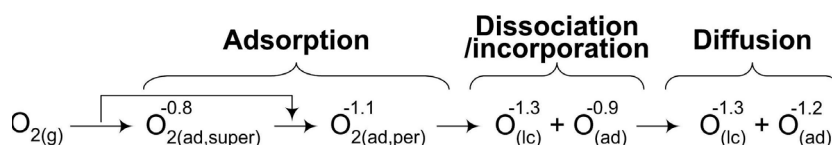


FIGURE 3. A Stepwise Reaction Mechanism of Oxygen Reduction on a Defective LMO Surface

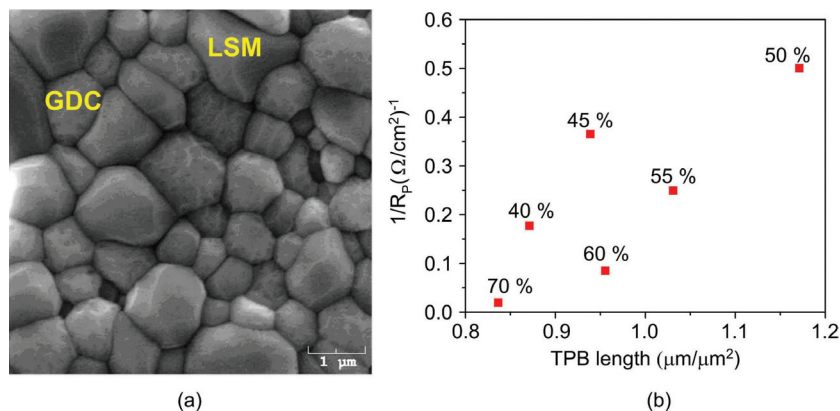


FIGURE 4. (a) SEM image of a dense LSM-GDC composite cathode fabricated by a co-pressing and co-sintering method. (b) Inverse polarization resistance versus TPB length. The values next to the data points are LSM volume percentages for the samples.

- Computer simulations on percolation for samples with various volume percentages will be performed to obtain a more complete picture of the amount of active TPB in order to better correlate with cell performance.
- Once the performance of the LSM-GDC composite electrode is well characterized, a thin film of another cathode material will be deposited on the composite cathode to determine its surface catalytic properties.

## FY 2007 Publications/Presentations

### Publications

- Y. M. Choi, D. S. Mebane, M. C. Lin, M. Liu, "Oxygen Reduction on LaMnO<sub>3</sub>-based Cathode Materials in Solid Oxide Fuel Cells," *Chemistry of Materials*, 19, 1690, 2007.
- D. S. Mebane, Y. Liu, M. Liu, "A Two-Dimensional Model and Numerical Treatment for Mixed-Conducting Thin Films: The Effect of Sheet Resistance," *Journal of the Electrochemical Society*, 154, A421, 2007.
- R. Williams Jr., S. Zha, M. Liu, "Fabrication and Characterization of Dense La<sub>0.85</sub>Sr<sub>0.15</sub>MnO<sub>3</sub>-Ce<sub>0.9</sub>Gd<sub>0.1</sub>O<sub>1.95</sub> Composite Electrodes," *Ceramic Engineering and Science Proceedings*, 2007.

4. Y. M. Choi, M. C. Lin, M. Liu, "Computational Study of Catalytic Mechanism toward Oxygen Reduction on  $\text{La}_{0.5}\text{Sr}_{0.5}\text{MnO}_3(110)$  in Solid Oxide Fuel Cells," *Angewandte Chemie, International Edition*, in press.
5. Y. M. Choi, D. S. Mebane, J. H. Wang, M. Liu, "Continuum and Quantum-Chemical Modeling of Oxygen Reduction on the Cathode in a Solid Oxide Fuel Cell," *Topics in Catalysis (Invited)*, in press.

### Presentations

1. R. Williams Jr., S. Zha, M. Liu, "Fabrication and Characterization of Dense  $\text{La}_{0.85}\text{Sr}_{0.15}\text{MnO}_3\text{-Ce}_{0.9}\text{Gd}_{0.1}\text{O}_{1.95}$  Composite Electrodes," 31<sup>st</sup> International Conference on Advanced Ceramics and Composites (ACerS), 2007.
2. Y. M. Choi, M. C. Lin, M. Liu "First-principles Investigation on Gas-Electrode Interactions in Solid Oxide Fuel Cells: Sulfur Tolerance and Oxygen Reduction Reaction," Exploratory Workshop-I/UCRC for Fuel Cells at USC-GT, Georgia, 2007.
3. Y. M. Choi, M. C. Lin, M. Liu "Computational Studies of the Oxygen Reduction Reaction on Cathode Materials for Solid Oxide Fuel Cells using Quantum-Chemical Calculations," 2<sup>nd</sup> Korea-USA Fuel Cell Symposium, South Carolina, 2007.

### References

1. Y. M. Choi, D. S. Mebane, J. H. Wang, M. Liu, "Continuum and Quantum-Chemical Modeling of Oxygen Reduction on the Cathode in a Solid Oxide Fuel Cell," *Topics in Catalysis (Invited)*, in press.
2. Y. M. Choi, D. S. Mebane, M. C. Lin, M. Liu, "Oxygen Reduction on  $\text{LaMnO}_3$ -based Cathode Materials in Solid Oxide Fuel Cells," *Chemistry of Materials*, 19, 1690, 2007.
3. Y. M. Choi, M. C. Lin, M. Liu, "Computational Study of Catalytic Mechanism toward Oxygen Reduction on  $\text{La}_{0.5}\text{Sr}_{0.5}\text{MnO}_3(110)$  in Solid Oxide Fuel Cells," *Angewandte Chemie, International Edition*, in press.
4. G. Kresse, J. Hafner, "Ab initio molecular dynamics for liquid metals," *Physical Review B*, 47, 558, 1993.
5. G. Kresse, J. Furthmüller, "Efficient iterative schemes for ab initio total-energy calculations using a plane-wave basis set," *Physical Review B*, 54, 11169, 1996.
6. E. A. Kotomin, R. A. Evarestov, Y. A. Mastrikov, J. Maier, "DFT plane wave calculations of the atomic and electronic structure of  $\text{LaMnO}_3(001)$  surface," *Phys. Chem. Chem. Phys.* 7, 2346, 2005.